PERGAMON

International Journal of Solids and Structures 37 (2000) 5353–5370

INTERNATIONAL JOURNAL OF SOLIDS and STRUCTURES

www.elsevier.com/locate/ijsolstr

Numerical analysis of crack-tip fields in functionally graded materials with a crack normal to the elastic gradient

Prabhakar R. Marur, Hareesh V. Tippur*

Department of Mechanical Engineering, Auburn University, Auburn, AL 36849, USA

Received 12 April 1999; in revised form 15 July 1999

Abstract

The nature of the singular field around the crack in functionally graded material (FGM) is analyzed parametrically using finite element method. The numerical simulations are carried out by varying the location of the crack in the graded region for different material gradients. Using linear material property variation in the gradient zone, the influence of material gradient and the crack position on the fracture parameters such as complex stress intensity factor (SIF) and energy release rate are studied. The crack opening displacement profiles of FGM are compared with the homogeneous and bimaterial counterparts. The analysis shows that the fracture parameters of FGM approach that of the bimaterial as the material gradient is increased, regardless of the position of the crack in the graded region. The extent of applicability of the homogenous crack tip fields around the crack in FGM is analyzed, and the results show that the size of the homogeneous field reduces with the increase in material gradient. Static fracture experiments are conducted on epoxy based FGM to determine complex SIF with electrical strain gages, using the homogeneous field equations to convert the strains to SIF. The measured SIF values compare favorably with the numerical results providing a limited experimental validation of the computations and the use of homogeneous field for FGM.

Keywords: Functionally graded material; Complex stress intensity factor; Energy release rate; Crack opening displacement; Numerical simulation; Electrical strain gages

1. Introduction

The requirement for advanced materials with high temperature resistance coupled with high toughness and thermal conductivity, has prompted research in the superalloy coating technology wherein the base material is clad with temperature resistant coatings. By the very nature of the principle of coating a

* Corresponding author. Fax: +1-334-844-3307.
E-mail address: htippur@eng.auburn.edu (H.V. Tippur).

0020-7683/00/$ - see front matter
PII: S0020-7683(99)00207-3

substrate, the coating material and the substrate have distinctly different chemical and thermo-mechanical properties. As a direct consequence, high residual stresses during the coating process and high thermal stresses in service are introduced. Hence, the interface between the substrate and the coating becomes a plane of weakness, and is prone to failures in service. Instead of coating a substrate or bonding two dissimilar materials with a plane of discontinuity, components may be produced with a progressive change in structure and properties (Niino et al., 1987). The material gradient eliminates the sharp interface and significantly relaxes the thermal stresses. Such nonhomogeneous material compositions are collectively referred to as functionally graded materials (FGMs).

The microstructure of FGM is generally heterogenous, and the dominant type of failure in FGM is the crack initiation and growth from the inclusions. Hence, the knowledge of crack growth and propagation is important in designing components involving FGM and improving its fracture toughness. Plane elasticity problems involving crack in FGM are solved by specifically assuming a functional form, usually a linear or an exponential function. Assuming an exponential spatial variation of the elastic modulus, Atkinson and List (1978), Dhaliwal and Singh (1978), and Delale and Erdogan (1983) solved crack problems for nonhomogeneous materials subjected to mechanical loads. By further assuming the exponential variation of thermal properties of the material, Jin and Noda (1993) and Erogan and Wu (1993) computed thermal stress intensity factor (SIF) for nonhomogeneous solids. Yang and Shih (1994) have obtained an approximate solution for an interlayer between two dissimilar materials from the known bimaterial solutions. Gu and Asaro (1997a) considered a semi-infinite crack in a strip of FGM under edge loading and obtained SIF relations for many commonly used fracture specimen configurations.

Recently, Erdogan (1995) has reviewed the elementary concepts of fracture mechanics of FGM and identified a number of typical problems relating to fracture of FGM. Eischen (1987) and Jin and Noda (1994) have shown that the singular field close to the crack-tip in a FGM is same as that of the homogeneous medium and the square root singularity is also preserved. Crack deflection in FGM has been considered by Gu and Asaro (1997b) who have reported the strong influence of material gradient on the crack kink angle when the crack is in the middle of the gradient zone. Tohgo et al. (1996) have carried out numerical analysis of particulate FGM, and studied the influence of material gradient on the size of singular field by comparing the FGM results with that obtained for homogeneous medium.

In this work, the influence of material gradient and crack location on the singular behavior of the stress and displacement fields is studied by comparing the numerical results with the solutions known for homogeneous and bimaterial cracks. Analysis of bimaterial interface cracks within the confines of linear elasticity theory leads to prediction of impractical oscillations in stresses and displacements. By considering the material gradients near the tip of the interface crack, the inadmissible oscillating behavior of the interface is removed. The motivation for modeling the material gradient at the crack-tip is the physical consideration that the diffusion and interpenetration in any bonding process would lead to very steep, nevertheless continuous variation of material parameters across the interface. Thus, the study of FGM would enhance the understanding of the fracture in a generic material, as the gradient layer in FGM upon shrinking is expected to behave like a sharp interface, and upon expansion, the fracture behavior would be analogous to a homogeneous material.

The basic field equations and the definitions of complex SIF and energy release rate in the context of a nonhomogeneous elastic medium are reviewed. The fracture behavior of FGM is characterized by energy release rate, complex SIF and crack opening displacement (COD). The fracture parameters are computed from the numerical results for different material gradients and crack positions within the gradient region. In the numerical simulations, linear material property variation is assumed as it closely matches the property variation in the FGM samples fabricated in this study. The details of the computational model, numerical results and static fracture experiments are presented in the following sections.

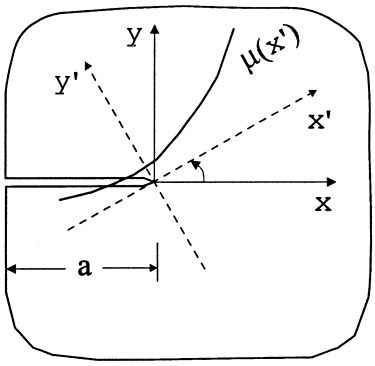

Fig. 1. Crack geometry in a general nonhomogeneous medium.

2. Crack-tip fields in FGM

Consider the plane elasticity problem of a finite crack lying in a medium with a general variation of the shear modulus μ, such as that shown in Fig. 1. The equation to be satisfied by the Airy's stress function ϕ is

$$\nabla^2\left(\frac{1}{E^*}\nabla^2\phi\right) - \frac{\partial^2}{\partial y^2}\left(\frac{1+\nu^*}{E^*}\right)\frac{\partial^2\phi}{\partial x^2} - \frac{\partial^2}{\partial x^2}\left(\frac{1+\nu^*}{E^*}\right)\frac{\partial^2\phi}{\partial^2 y} + 2\frac{\partial^2}{\partial x\,\partial y}\left(\frac{1+\nu^*}{E^*}\right)\frac{\partial^2\phi}{\partial x\,\partial y} = 0, \tag{1}$$

where E^*, ν^* are given by E, ν under plane stress conditions and by $E/(1-\nu^2)$, $\nu/(1-\nu)$ under plane strain conditions, E is Young's modulus, ν is Poisson's ratio and ∇^2 is the Laplacian operator. Upon expanding the above equation, the first term in the governing differential equation for ϕ involves the biharmonic term identical to the homogeneous material, while the remaining terms involve the spatial derivatives of the elastic moduli (Eischen, 1987). Hence, the elastic stress and displacement fields can be derived using the stress function in variable separable form, identical to the homogeneous case. Hence, the singular stresses near the crack tip can be given as

$$\sigma_{ij} \cong \frac{1}{\sqrt{2\pi r}}\left[K_{\mathrm{I}} f^{\mathrm{I}}_{ij}(\theta) + K_{\mathrm{II}} f^{\mathrm{II}}_{ij}(\theta)\right], \quad i,j = x,y, \tag{2}$$

where K_{I} and K_{II} are the mode-I and mode-II SIFs, respectively, and $f^{\mathrm{I}}_{ij}(\theta)$ and $f^{\mathrm{II}}_{ij}(\theta)$ are the standard angular functions for a crack in homogeneous elastic medium.

Although the material gradient does not influence the square-root singularity or the singular stress distribution, the material gradient affects the size of the region in which the homogeneous solution is valid. This differs from the case of homogeneous material in which the material property does not enter the stress field of a traction problem. The nature of stress field of FGM also differs from the bimaterial case in which the near tip stresses have oscillating singularity, and both SIF and angular functions involve material properties reflected via mismatch parameter ϵ as:

$$\sigma_{ij} \sim \frac{1}{\sqrt{r}}\left[K_1 \sum\nolimits^{\mathrm{I}}_{ij}(\theta, \ln r; \epsilon) + K_2 \sum\nolimits^{\mathrm{II}}_{ij}(\theta, \ln r; \epsilon)\right], \quad i,j = x,y, \tag{3}$$

where $\sum^{\mathrm{I}}_{ij}$ and $\sum^{\mathrm{II}}_{ij}$ are the angular functions.

When the crack is not parallel to the material gradient, the response of the crack in a FGM is always

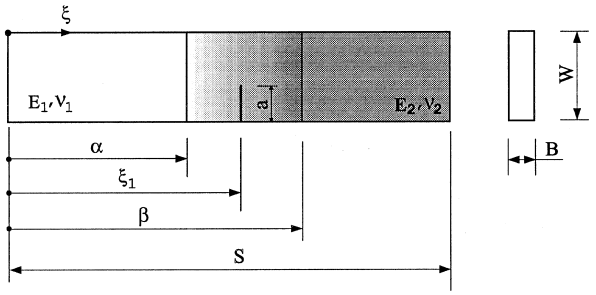

Fig. 2. Parametric model of the FGM.

mixed mode regardless of the remote loading conditions due to the lack of symmetry in the material properties. Hence, the complex SIF for FGM can be defined as $K_I + \imath K_{II}$, and the mode-mixity ψ can be given as $\tan^{-1}(K_{II}/K_I)$. Due to the regular singularity of the crack tip fields in FGM, the mode-mixity definition does not require an arbitrary length parameter in contrast to the bimaterial crack.

The energy release rate for a crack in FGM is given by

$$G = \frac{1}{E^*}\left(K_I^2 + K_{II}^2\right), \tag{4}$$

where E^* is E_0 for plane stress and $E_0/(1-\nu_0^2)$ for plane strain; and E_0 and ν_0 are the limit values of

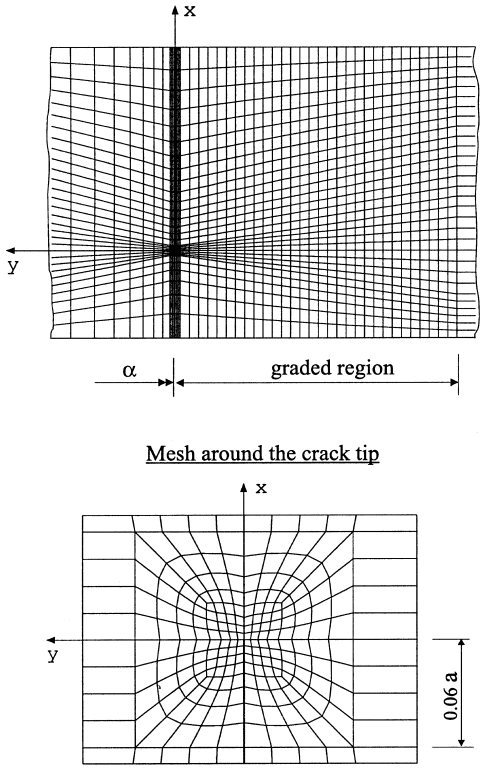

Fig. 3. Finite element mesh for crack positioned at $\xi_1 = \alpha$.

Young's modulus and Poisson's ratio, respectively, at the crack tip. It must be noted that this definition of G is same as that for the homogeneous material, and is independent of the orientation of the crack or the form of material property variation.

3. Computational model

The conventional isoparameteric finite elements are used for modeling the FGM. A very fine rectangular mesh is used to adequately model the singularity and also the material property gradients. For facilitating the finite element modeling and for notational convenience, the FGM specimen is divided into three regions: the gradient region and the homogeneous regions on either side of the gradient part as shown in Fig. 2. The boundaries of these regions are marked by dimensionless variables using the normalized coordinate ξ. In Fig. 2, the model is bimaterial if $\alpha = \beta$, and is homogeneous if $\alpha = 1$. The position of the crack is marked by ξ_1, which can take a value from α through β.

A pre-processor program for the finite element analysis (FEA) software has been written, with which the parameters α, β and ξ_1 can be varied. Based on the user-defined parameter values, the pre-processor code generates a rectangular mesh with eight-noded isoparameteric elements with 2 dof (degrees of freedom) at each node. The elements in the gradient region are grouped into narrow parallel strips parallel to the crack to facilitate material property modification. In all the models used in the parametric study, the material gradient is achieved by subdividing the graded region into 30 strips of elements with linear material property variation. The finite element mesh with the crack positioned at α is shown in Fig. 3, which contains 1928 elements and 5993 nodes.

The magnitude and phase of complex SIF are computed by extrapolating the nodal displacements extracted from the FEA. The displacement equations of the bimaterial crack are used in the formulation to relate the nodal displacements to the complex SIF. This technique is unified for all the material types, namely, homogeneous, bimaterial and FGM, and it has been calibrated for static and dynamic loading conditions by Marur and Tippur (1998) and Marur (1999).

The energy release rate is computed using the standard J-integral formulation. Smelser and Gurtin (1977) have shown that the J-integral can be extended without modifications to interface crack in a bimaterial provided the crack is straight. In the case of the FGM, the path independence of the J-integral holds only for the case of crack being normal to the direction of material property variation. For general material property variation in relation to the direction of the crack, additional terms must be included in the formulation as shown by Honein and Hermann (1997).

4. Analysis of fracture parameters

The geometry used for the parametric simulations is an edge-cracked specimen with uniform tensile stress σ_0 applied at the boundaries. The ratio of upper and lower limits of Young's modulus is 3 and Poisson's ratio is constant at 0.35. In the numerical implementation, the interface between the gradient region and the compliant material is marked by α and the 'stiffer interface' is marked by β. The dimensions of the model simulated are: $S = 6W$, $W = 4B$ and $B = 6.25$ mm.

For a given combination of two bulk materials, the crack in FGM is expected to behave like bimaterial interface crack if the gradient zone denoted by $(\beta - \alpha)$ approaches zero and would be analogous to a homogeneous crack if the graded zone is made large enough. Hence, the parametric simulations are carried out by varying $(\beta - \alpha)$ for different crack positions inside the graded region. Three distinct crack locations are chosen: $\xi_1 = \alpha$, $\xi_1 = (\beta - \alpha)/2$ and $\xi_1 = \beta$. For each combination of

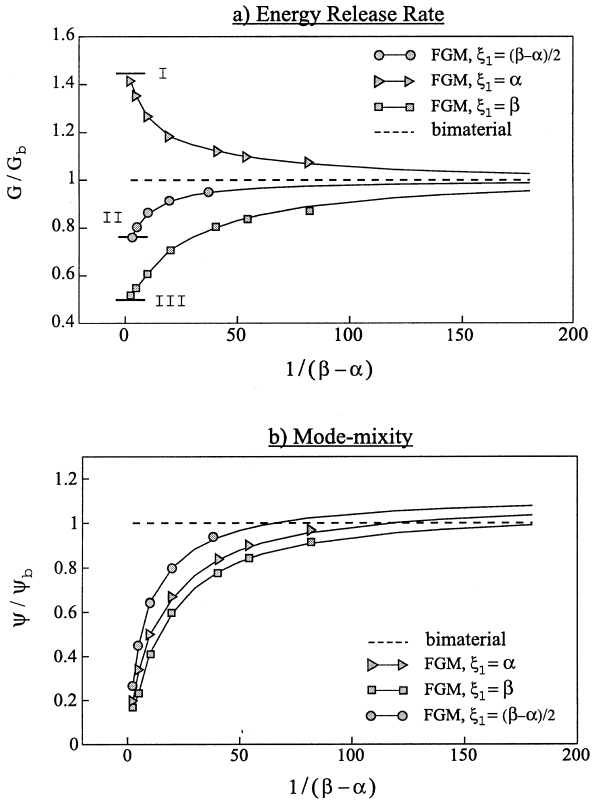

Fig. 4. The variation of G and ψ with material gradient. The labels I, II and III represent the G of homogenous cracks with E same as that at α, $(\beta-\alpha)/2$ and β, respectively.

gradient zone size and crack position, the energy release rate, mode-mixity, complex SIF and COD are computed.

4.1. Energy release rate

The energy release rate and mode-mixity for different material gradients are computed by reducing $(\beta-\alpha)$ in steps. Due to excessive element distortion, the gradient zone could not be reduced beyond 2% of the total length of the specimen and the energy release rate and mode-mixity for the case of $(\beta-\alpha)$ approaching zero are obtained by polynomial extrapolation. The variations of energy release rate (normalized by the energy release rate of a corresponding bimaterial crack, G_b) for the three crack positions are plotted in Fig. 4(a). The abscissa reflects the material gradient, where the origin represents homogeneous case and infinity represents a jump in material property (bimaterial case). The energy release rates for homogeneous materials with Young's modulus corresponding to the Young's modulus at three different crack positions in FGM are also shown in the figure. It can be observed from the figure that the energy release rate of the FGM starts from the corresponding homogeneous value and approaches the bimaterial value as the material gradient is increased. The rate of approach is different for different crack positions.

The variation of mode-mixity (normalized by the mode-mixity of the bimaterial crack, ψ_b) is shown in Fig. 4(b). The mode-mixity of FGM approaches the bimaterial value asymptotically as the material

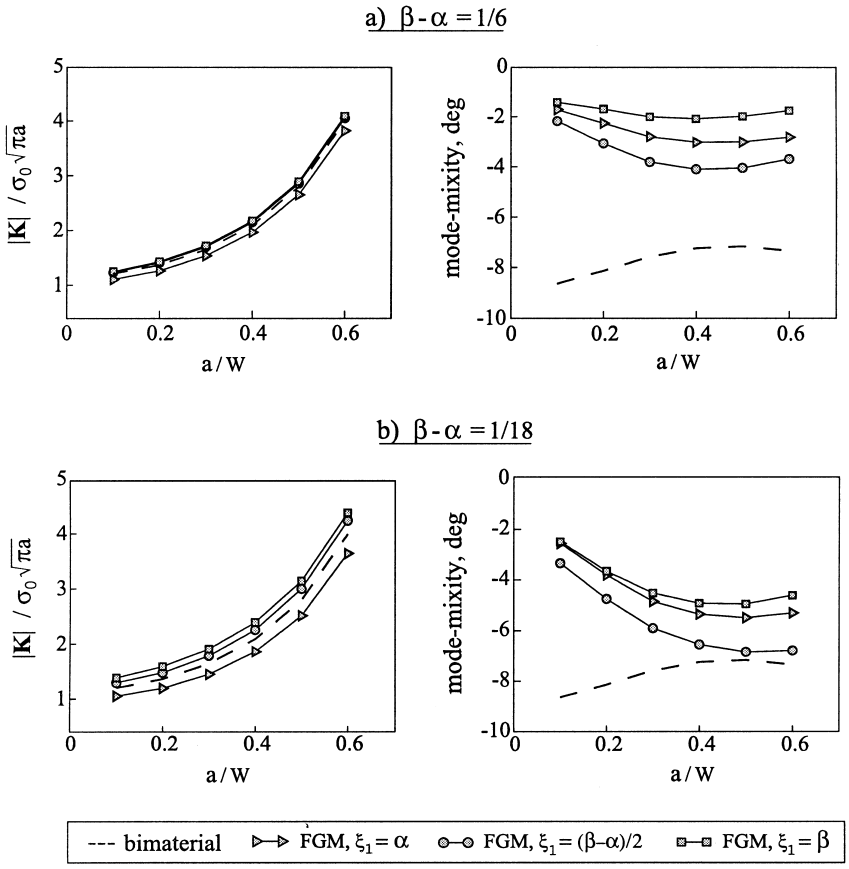

Fig. 5. Variation of magnitude of SIF and mode-mixity with crack length.

gradient is increased. The mode-mixity curves flatten out after a sharp increase from the base value in all the three cases. It must be remarked that the mode-mixity of bimaterial is defined using an arbitrary length parameter (which is set to $2a$ in this study) which renders the mode-mixity of bimaterial non-unique. However, the length parameter has a weak influence on the computed mode-mixity, which is in line with the analytical results published by Rice (1988).

As could be observed from Fig. 4, the crack at the middle of the gradient region closely follows the bimaterial case. For any given size of the gradient region (alternatively, the material gradient), the crack positioned at the middle of the graded region has the energy release rate closest to the bimaterial value, and has the highest mode-mixity among the crack positions.

4.2. Complex stress intensity factor

The magnitude and phase angle of complex SIF for different crack lengths, for two sizes of the gradient region, $\beta - \alpha = 1/6$ and $1/18$, are plotted in Fig. 5. The magnitude of SIF is normalized by $\sigma_0\sqrt{\pi a}$, where σ_0 is applied remote tensile stress and a is the crack length. From the figure, it can be seen that the magnitude of SIF is about the same for various material types and significant differences are seen in the mode-mixity values. For any given a/W ratio, the mode-mixity of FGM increases substantially with the reduction in the gradient region, which is in line with Fig. 4 where monotonic

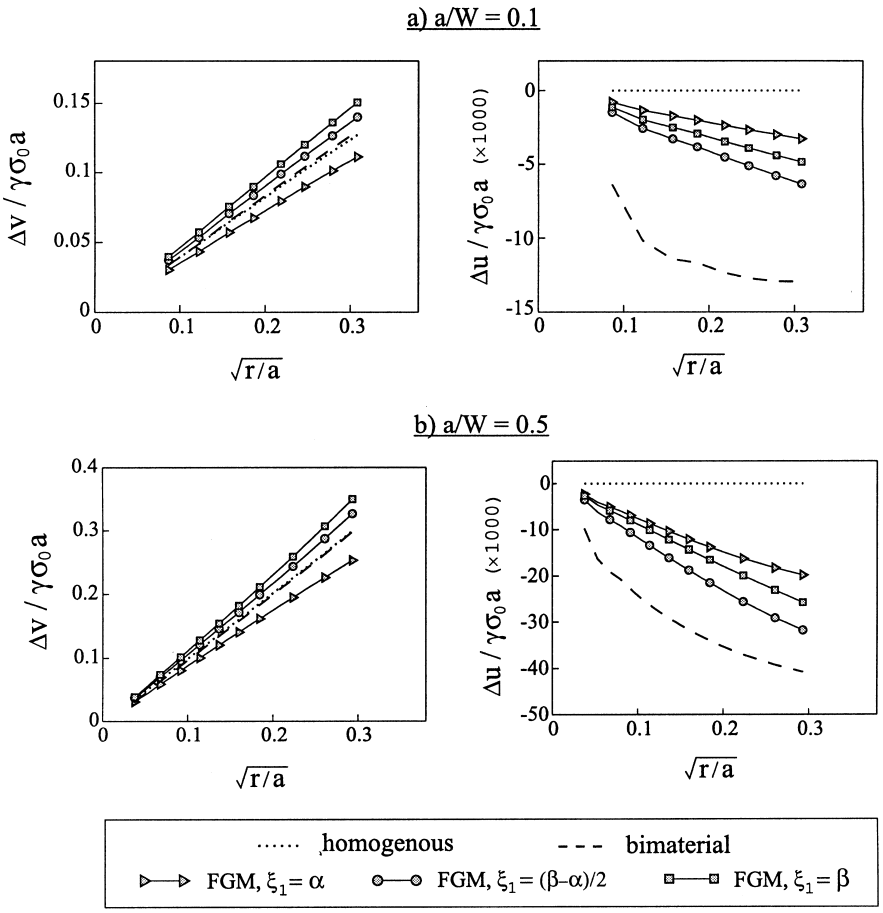

Fig. 6. Crack opening and sliding displacement profiles for different crack lengths for the gradient zone size of $(\beta - \alpha) = 1/18$.

increase in the magnitude of mode-mixity with decrease in $(\beta - \alpha)$ is shown. As observed in the previous section, the crack positioned at the middle of the gradient zone closely follows the bimaterial case.

At low a/W ratios, the mixity values for the bimaterial crack and FGM crack are distinctly different, and they approach a common value as the a/W ratio is increased. In FGM, the mode-mixity increases with a/W ratio, regardless of the position of the crack in the gradient region. This is in contrast to bimaterial crack, wherein the mode-mixity decreases with the crack length.

Since the magnitude of SIF is about the same for cracks in both FGM and bimaterial, the variation in mode-mixity comes from the mode-II contribution. Thus, the mode-II SIF is influenced more by the material gradient. This observation is in consonance with the analytical results published by Gu and Asaro (1997b), who have shown that K_{II} is strongly dependent on the material gradient.

4.3. Crack opening displacement

The crack face displacements in different material systems for two a/W ratios, 0.1 and 0.5, are analyzed in this section. The gradient zone size is same at 1/18 of the specimen length for the FGM. The displacements of nodes lying in the region prescribed by r from $0.01a$ to $0.1a$ are used in the

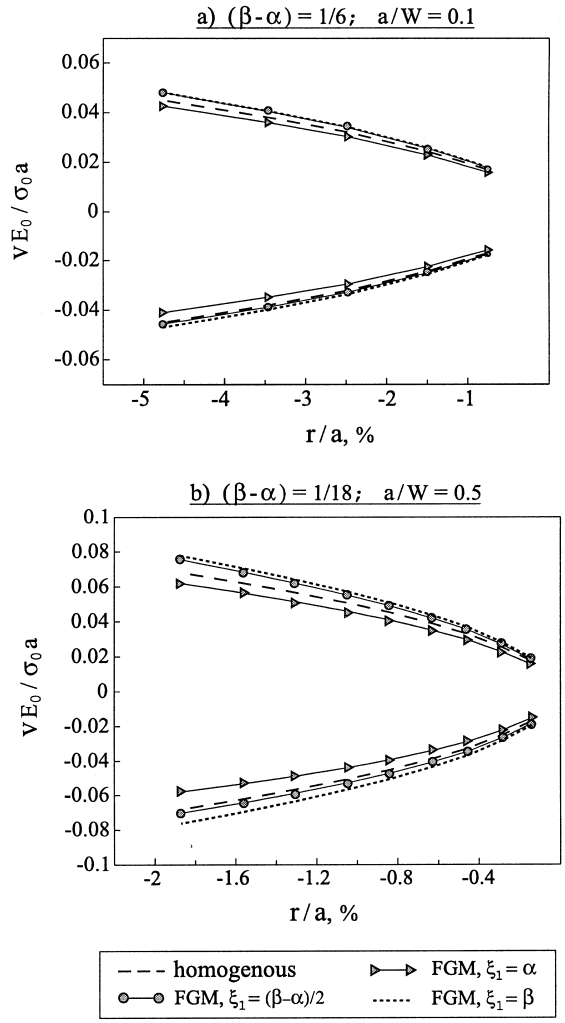

Fig. 7. Comparison of COD profile of homogeneous material with FGM.

computations. From the nodal displacements, the opening and sliding displacement jump across the crack faces, denoted by Δv and Δu respectively, are computed. Fig. 6 shows the sliding and opening displacements normalized by $\gamma\sigma_0 a$, where

$$\gamma = \left|\frac{c_1 + c_2}{2\sqrt{\pi}(1 + 2\imath\epsilon)\cosh(\pi\epsilon)}\right|, \tag{5}$$

$\imath = \sqrt{-1}$, $c_j = (1 + \kappa_j)/\mu_j$, $\kappa_j = 3 - 4\nu_j$ for plane strain and $\kappa_j = (3 - \nu_j)/(1 + \nu_j)$ for plane stress. The subscript j takes the value of 1 and 2 corresponding to material 1 and 2, respectively. From the figure, it can be seen that the crack opens by different magnitudes depending on the material type, and the differences in Δv among the material types are not as significant as in Δu. With the increase in a/W ratio, the sliding displacement of FGM increases and approaches that of the bimaterial crack.

With the COD plots shown in Fig. 6, the variation of complex SIF with material gradient discussed in

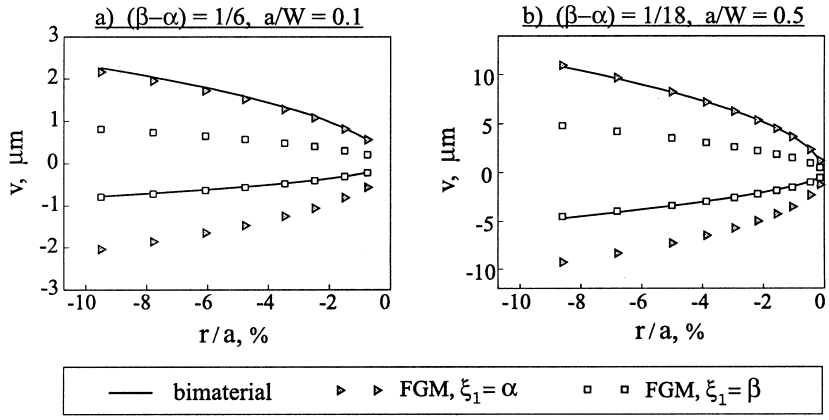

Fig. 8. Comparison of COD profile of bimaterial with FGM.

the previous section can be explained. In the case of bimaterial crack, Δv and Δu reflect the strength of K_1 and K_2, respectively. For homogeneous and gradient materials, the crack face displacements relate to mode-I and mode-II SIF through

$$\Delta v(r) = \frac{1+\kappa}{2\pi\mu} K_{\mathrm{I}} \sqrt{2\pi r},$$

$$\Delta u(r) = \frac{1+\kappa}{2\pi\mu} K_{\mathrm{II}} \sqrt{2\pi r}. \tag{6}$$

As the sliding displacements are more sensitive to elastic gradients, mode-II SIF is, consequently, strongly influenced by the gradients in the elastic properties.

The opening and sliding displacements are linear in $\sqrt{r}$ for the homogeneous and FGM cases as could be noted in Eq. (6). In Fig. 6, the variation of Δv is quite linear for all the material types except for the case of crack positioned at $\xi_1 = \alpha$ in the FGM, which has nonlinearity at larger radius from the crack-tip. The variation of Δu for cracks in FGM is linear for most part of r/a values considered, except for the crack positioned at $\xi_1 = \alpha$.

The nature of variation of opening and sliding displacement with radial distance clearly shows that the sliding displacement is the factor that distinguishes the crack at a sharp interface from that at a graded interface. Alternatively, this can be stated that mode-mixity is the key parameter that distinguishes the nature of the interface crack. To gain further insight into the crack face deformations in FGM, the crack opening profiles of FGM are compared with the homogeneous and bimaterial cracks in the following sections.

4.3.1. Comparison with homogeneous material

The crack opening profiles for different crack positions in FGM are compared with that of the homogeneous medium in Fig. 7. The crack face displacements are normalized by $\sigma_0 a/E_0$, where E_0 is the Young's modulus at the crack-tip. The crack opening profiles for the three crack positions are different and asymmetric, and are also different from the symmetric homogeneous case. This variation is due to the differences in mode-mixities, although the angular distribution of stresses and displacements of FGM are identical to the homogeneous case.

Contrary to the expectation, the deformations for the crack positioned at the compliant boundary of

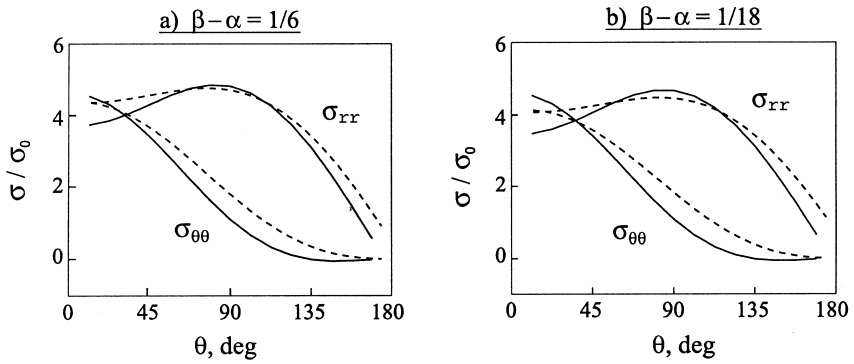

Fig. 9. Comparison of *K*-domiant stress fields with numerical data for crack at ($\xi_1 = \alpha$). ——— *K*-dominant solution, ——— FEA.

the graded zone are lesser than the corresponding homogeneous crack. The opposite holds true for the crack positioned at the stiffer interface. This phenomenon is not apparent from the asymptotic displacement equations for FGM.

4.3.2. Comparison with bimaterial

The crack opening profiles for the cracks positioned at the stiff and compliant interfaces in FGM are compared with that of the corresponding bimaterial crack in Fig. 8. The upper crack flank of the bimaterial nearly coincides with the upper flank of FGM with the crack at the compliant interface, and the lower crack flank of bimaterial matches with the lower flank of FGM crack at the stiffer interface. The matching of crack opening profiles is seen in both the cases where the gradient zone sizes differ by a factor of 3 and the a/W ratios vary by a factor of 5. In the limit the gradient region is removed, the upper and lower crack flanks of FGM and bimaterial would coincide.

4.4. Singular stress field

In this section, the numerical stress data obtained from the FEA of FGM are compared with the analytical homogeneous crack-tip solution. The region of validity of the homogeneous crack-tip solution in FGM is also investigated. As fracture experiments are conducted on FGM with the crack position at

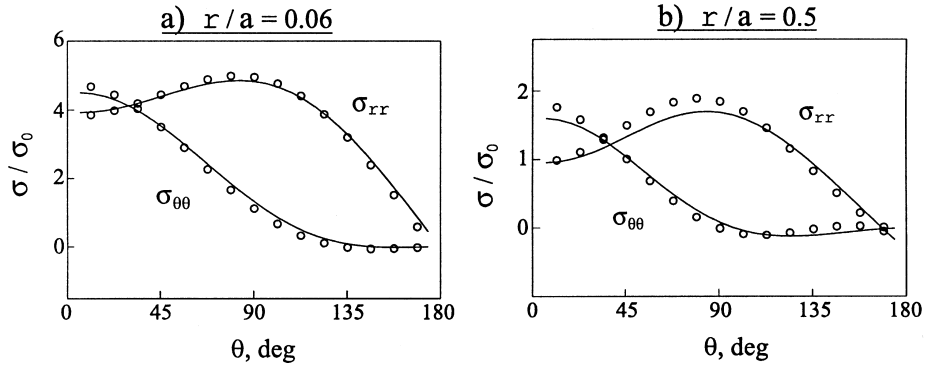

Fig. 10. Angular stress distribution at different radii. ($\beta - \alpha = 1/6$); crack at ($\xi_1 = \alpha$). ○ series solution with eight-terms, ——— FEA.

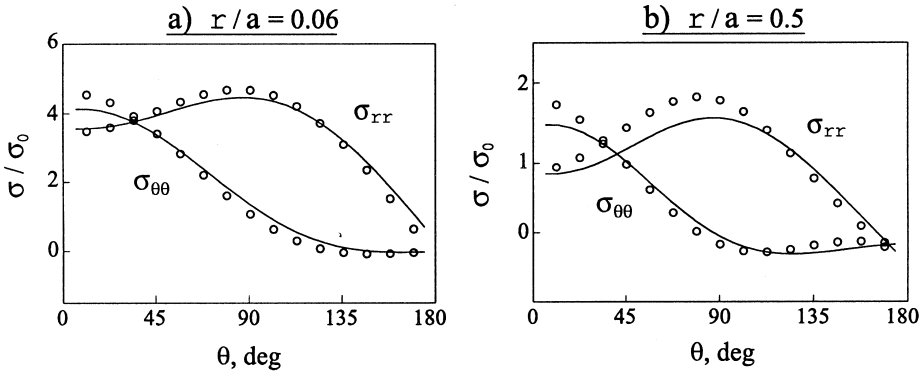

Fig. 11. Angular stress distribution at different radii. ($\beta - \alpha = 1/18$); crack at ($\xi_1 = \alpha$). ○ series solution with eight-terms, ——— FEA.

$\xi_1 = \alpha$, only this configuration is analyzed. Two gradient zone sizes, $\beta - \alpha = 1/6$ and $1/18$, are chosen, while maintaining the a/W ratio at 0.3 in both cases. The stresses along two different radii $r/a = 0.06$ and 0.5, are used in the comparison.

It is usually presumed that the asymptotic homogeneous fields are valid close to the crack-tip in FGM. However, the K-dominant solution does not provide a good match for FEA results even for a low r/a ratio of 0.06 as illustrated in Fig. 9. Higher-order terms of the series solution are needed to bring about a good agreement between the analytical and numerical results. The coefficients of the higher-order terms are obtained by solving the homogeneous version of the finite element model shown in Fig. 3. Two sets of coefficients are obtained by solving for pure mode-I and mode-II loading cases. The two sets of coefficients are multiplied by the individual components of the complex SIF of FGM and are linearly superposed to obtain the analytical stress distribution as described in Appendix A.

The finite element results are compared with the homogeneous series solution, obtained with first eight-terms of the series, in Figs. 10 and 11. At low r/a ratios, the match between the numerical results and the homogeneous series solution is quite good for both the gradient zone sizes. However, as the radial distance is increased, the match between the two is less satisfactory. The mismatch is more pronounced for steeper material gradients. Increasing the number of higher-order terms beyond eight in the analytical solution did not result in any perceptible improvement in the agreement between the numerical and analytical solutions. Hence, the mismatch of the numerical and analytical results could be due to the invalidity of homogeneous solution in FGM at the radial distance being considered.

An approximate estimate of the region in which the homogeneous asymptotic solution is applicable for a crack in FGM has been derived by Jin and Batra (1996). Neglecting the gradients of Poisson's ratio, Jin and Batra (1996) have shown that the homogeneous crack-tip solution will be valid in the region where the following inequalities are satisfied:

$$\frac{1}{E_0}\frac{\partial E}{\partial x} \ll \frac{1}{r}, \quad \frac{1}{E_0}\frac{\partial^2 E}{\partial x\,\partial y} \ll \frac{1}{r^2}. \tag{7}$$

For unidirectional variation of material properties, it is suffice to satisfy the first inequality in the above equation. For the gradient zone sizes of $\beta - \alpha = 1/6$ and $1/18$, the numerical estimates for r/a can be obtained as

$$\frac{r}{a} \ll 1.1, \quad \frac{r}{a} \ll 0.37, \tag{8}$$

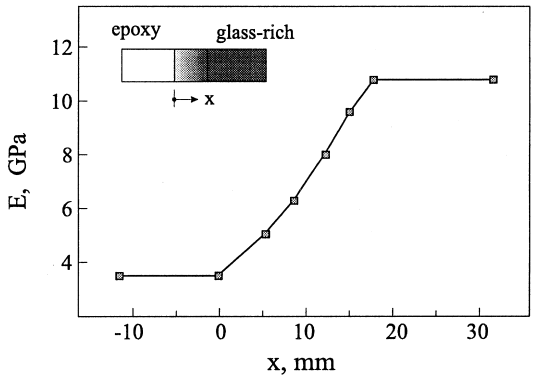

Fig. 12. Variaton of static Young's modulus of the FGM specimen.

respectively. For $\beta - \alpha = 1/6$, the ratio r/a should be far less than 1.1 for the homogeneous solution to be valid. In Fig. 10(b), the normalized radius of 0.5 is lesser than 1.1, although not far less than 1.1 as required by first inequality, the homogeneous solution provides a reasonable fit to the finite element results. In the case of $\beta - \alpha = 1/18$, the normalized radius of 0.5 is more than the limit prescribed by Eq. (8) for this gradient, resulting in poor match between the analytical and numerical results.

5. Experiments

Static fracture experiments are conducted on epoxy based FGM samples with the crack positioned at the compliant side ($\xi_1 = \alpha$). The FGM specimens are fabricated using the gravity-assisted casting technique (Marur and Tippur, 1998) with two-part slow curing epoxy and uncoated solid glass sphere fillers. This casting technique has been successful in producing FGMs with gradient region from 15 to 21 mm in length, with consistent material properties. The variation of elastic properties in the FGM sample is determined by mounting strain rosettes along the length of the specimen and loading the specimen in cantilever configuration with dead weights. Young's modulus is obtained from the slope of load versus longitudinal strain plot, and Poisson's ratio is computed from the ratio of transverse to longitudinal strain. The variation of Young's modulus in the gradient region is shown in Fig. 12. It can be observed from the figure that the variation of modulus within the gradient region is quite linear. The

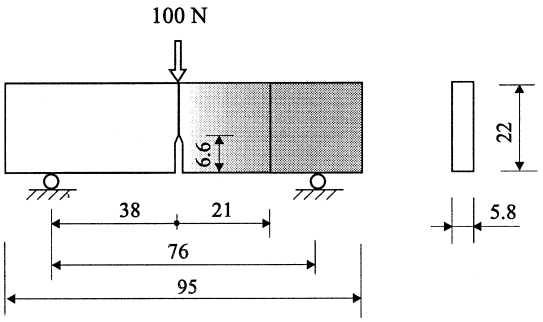

Fig. 13. Specimen geometry. All dimensions in mm.

Poisson's ratio variation is also linear within the graded zone, with the upper and lower limits at 0.35 and 0.28 for epoxy and glass-rich sides, respectively.

The samples are machined to the final dimensions as shown in Fig. 13. The specimen is loaded in three point bend configuration under 100 N midspan load. A 0.81 mm biaxial strain rosette (CEA-13-032WT-120 from Measurements Group Inc.) is mounted at $r = 3.5$ mm from the crack tip at an angle of 90° as described in Appendix B. The upper limit of the radius of valid zone predicted by Eq. (7) for this specimen is 10.5 mm. Since the strain gage is located well within this prescribed region, the homogeneous crack-tip solution is expected to be valid. The measured radial and hoop strains are converted to complex SIF data using the formulation described in Appendix B. The SIF computed from the strain data are $|\mathbf{K}| = 0.65$ MPa $\mathrm{m}^{1/2}$ and $\psi = -3.45°$, while the finite element results are $|\mathbf{K}| = 0.59$ MPa $\mathrm{m}^{1/2}$ and $\psi = -3.24°$. The good agreement between the numerical and measured data provides a limited experimental validation of the applicability of the homogenous stress field around the crack in FGM.

6. Discussion

The fracture parameters of FGM starting from the homogenous values approach the bimaterial values as the material gradient is increased. The rate of approach to the bimaterial values is dependent on the position of the crack within the gradient region. The crack at the middle of the gradient region closely follows the bimaterial case in terms of the energy release rate and the mode-mixity.

The variation of magnitude and phase of complex SIF of FGM with crack length for two different material gradients are studied. The magnitude of SIF is comparable to that of the bimaterial crack, while significant differences are seen in the mode-mixity values. With the increase in crack length, the mode-mixity of FGM increases regardless of the position of the crack in the graded region. In contrast, the mode-mixity decreases with a/W ratio for bimaterial crack. For a given crack length, the mode-mixity of FGM cracks ultimately reach the bimaterial value as the material gradient is increased. However, at low a/W ratios, typically below 0.2, there is a substantial difference in the mode-mixity values of FGM and bimaterial.

The COD profiles of cracks positioned at different planes in FGM are different and none of them match with that of the homogenous crack. This variation is due to the differences in mode-mixity for different crack positions in the graded region, although the asymptotic fields are identical in all the cases. The crack positioned at the compliant boundary in FGM has lesser COD than a corresponding homogenous crack, and the opposite holds true for the crack positioned at the stiffer boundary. The reasoning for this unintuitive behavior could not be advanced as generic full-field solutions are not currently available in the literature. The deformed upper and lower crank flanks of bimaterial coincide with the upper and lower crack flanks of the cracks positioned at the boundaries of compliant and stiff sides of FGM, respectively. In the limit the gradient zone is removed, the COD of FGM would be identical to that of the bimaterial.

The angular stress distributions at different radii around the crack tip are obtained from the FEA data, and are compared with the homogenous crack-tip solution. The results show that although the homogenous solution is valid close to the crack-tip, the K-dominant terms provide a poor match to the numerical results. Higher-order terms are needed to achieve a good agreement between the analytical and numerical solution within the region where the homogenous crack-tip solution is valid. The relations proposed by Jin and Batra (1996) provide a good estimate of the size of the homogeneous field around the crack in FGM.

7. Conclusions

The singular field around a crack in FGM with linear property variation is parametrically studied, and the fracture parameters are compared with that of the homogeneous and bimaterial cracks. The geometric parameters, namely the position of the crack within the gradient zone, size of the gradient region and the crack length are varied. For each combination of the parameters, the energy release rate, complex SIF, mode-mixity and CODs are computed. The crack in FGM, regardless of the position in the graded zone, approach the bimaterial crack behavior as the gradient is increased. Among the crack positions considered, the crack at the middle of the graded zone has characteristics that are closest to the bimaterial cracks. The mode-II SIF is strongly influenced by the material gradient and the crack position, and this is apparent from the strong dependence of sliding displacements of the crack flanks on the material gradient. The size of the singular field reduces with the increase in the material gradient and K-dominant terms of the series solution do not describe the field adequately even close to the crack-tip. Static fracture experiments are conducted on epoxy based FGM to determine complex SIF using electrical strain gages. The SIF values estimated from the measured strains compared favorably with numerical results providing a limited experimental validation of the numerical results.

Acknowledgements

The support of National Science Foundation under grant number CMS-9622055 is gratefully acknowledged. The first author would like to thank his family for providing support during the course of this investigation.

Appendix A. Computation of mixed-mode stress field

To describe the mixed-mode stress field around the crack-tip in FGM, the coefficients of the series solution for the homogeneous medium must be determined. As mode-mixity changes with the material gradient, the coefficients must be evaluated for each specimen configuration. The complete solution of each specimen configuration as a boundary value problem is a laborious and time-consuming process, especially for parametric analysis. In this study, a simple solution is proposed to compute the mixed-mode stress field by method of superposition. Two sets of coefficients are computed corresponding to the pure mode-I and mode-II loading cases. Once the series coefficients are known, the stress field for any mode-mixity can be computed by linear superposition as described below.

The complete series solution for the stress field around a crack lying in a homogeneous elastic medium can be given as

$$\begin{aligned}\sigma_{rr} = \sum_{n=0}^{N} &\mathscr{R}(\mathbf{A}_n) r^{n-1/2}\left[\cos\hat{\theta}_1 + \cos\theta_1 + (1-2n)\sin\theta\sin\hat{\theta}_2\right] + \mathscr{J}(\mathbf{A}_n) r^{n-1/2}\left[3\sin\hat{\theta}_1 + \sin\theta_1 - (1\right.\\ &\left. - 2n)\sin\theta\cos\hat{\theta}_2\right] + 2\mathscr{R}(\mathbf{B}_n) r^{n}\left[\cos n\theta + \cos(n+2)\theta - n\sin\theta\sin(n+1)\theta\right] + 2\mathscr{J}(\mathbf{B}_n) r^{n}\left[\right.\\ &\left. - \sin n\theta - n\sin\theta\cos(n+1)\theta\right], \end{aligned} \tag{A1}$$

$$\sigma_{\theta\theta} = \sum_{n=0}^{N} \mathscr{R}(\mathbf{A}_n) r^{n-1/2} \left[3\cos\hat{\theta}_1 - \cos\theta_1 - (1-2n)\sin\theta\sin\hat{\theta}_2 \right] + \mathscr{I}(\mathbf{A}_n) r^{n-1/2} \left[\sin\hat{\theta}_1 - \sin\theta_1 \right.$$
$$\left. + (1-2n)\sin\theta\cos\hat{\theta}_2 \right] + 2\mathscr{R}(\mathbf{B}_n) r^n \left[\cos n\theta - \cos(n+2)\theta + n\sin\theta\sin(n+1)\theta \right]$$
$$+ 2\mathscr{I}(\mathbf{B}_n) r^n \left[-\sin n\theta + n\sin\theta\cos(n+1)\theta \right], \tag{A2}$$

where

$$\theta_1 = (n - 1/2)\theta,$$

$$\theta_2 = (n - 3/2)\theta,$$

$$\hat{\theta}_j = \theta_j + 2\theta, \quad j = 1, 2,$$

and $\mathbf{A}_n$ and $\mathbf{B}_n$ are complex coefficients. The coefficient of the first term in the series is related to the complex SIF ($= K_{\mathrm{I}} + \imath K_{\mathrm{II}}$) through

$$\mathbf{K} = 2\sqrt{2\pi}\bar{\mathbf{A}}_0. \tag{A3}$$

The stress distribution is fully defined once the complex coefficients are determined. The coefficients can be obtained from optical measurements or can be computed using numerical methods. In this study, the coefficients are computed using least-squares analysis of finite element data as described in Ref. (Marur, 1999).

Two sets of coefficients, $\mathbf{A}_n^{\mathrm{I}}$ and $\mathbf{B}_n^{\mathrm{I}}$, $\mathbf{A}_n^{\mathrm{II}}$ and $\mathbf{B}_n^{\mathrm{II}}$, where the superscripts I and II correspond to pure mode loading cases with ($K_{\mathrm{I}} = 1$ and $K_{\mathrm{II}} = 0$) and ($K_{\mathrm{I}} = 0$ and $K_{\mathrm{II}} = 1$), respectively, are evaluated. In addition, for each FGM specimen type, the complex SIF is computed using the nodal extrapolation technique. Then, the series coefficients for the mixed-mode field can be computed as

$$\mathbf{A_n} = K_{\mathrm{I}}\mathbf{A}_n^{\mathrm{I}} + K_{\mathrm{II}}\mathbf{A}_n^{\mathrm{II}}, \tag{A4}$$

$$\mathbf{B_n} = K_{\mathrm{I}}\mathbf{B}_n^{\mathrm{I}} + K_{\mathrm{II}}\mathbf{B}_n^{\mathrm{II}}. \tag{A5}$$

By substituting these 'scaled' coefficients in Eqs. (A1) and (A2), the radial and hoop stress distribution can be obtained.

Appendix B. Strain to SIF formulation

With a plane stress assumption, the strain field around a crack in homogeneous medium can be given as

$$\epsilon_{rr} = \frac{1}{E_0\sqrt{2\pi r}} \left[K_{\mathrm{I}} \left(f^{\mathrm{I}}_{rr} - \nu_0 f^{\mathrm{I}}_{\theta\theta} \right) + K_{\mathrm{II}} \left(f^{\mathrm{II}}_{rr} - \nu_0 f^{\mathrm{II}}_{\theta\theta} \right) \right] + O(r), \tag{B1}$$

$$\epsilon_{\theta\theta} = \frac{1}{E_0\sqrt{2\pi r}} \left[K_{\mathrm{I}} \left(f^{\mathrm{I}}_{\theta\theta} - \nu_0 f^{\mathrm{I}}_{rr} \right) + K_{\mathrm{II}} \left(f^{\mathrm{II}}_{\theta\theta} - \nu_0 f^{\mathrm{II}}_{rr} \right) \right] + O(r), \tag{B2}$$

where

$$f^{\mathrm{I}}_{rr}(\theta) = \left[\frac{5}{4}\cos\frac{\theta}{2} - \frac{1}{4}\cos\frac{3\theta}{2}\right],$$

$$f^{\mathrm{II}}_{rr}(\theta) = \left[\frac{-5}{4}\sin\frac{\theta}{2} + \frac{3}{4}\sin\frac{3\theta}{2}\right],$$

$$f^{\mathrm{I}}_{\theta\theta}(\theta) = \left[\frac{3}{4}\cos\frac{\theta}{2} + \frac{1}{4}\cos\frac{3\theta}{2}\right],$$

$$f^{\mathrm{II}}_{\theta\theta}(\theta) = \left[\frac{-3}{4}\sin\frac{\theta}{2} - \frac{3}{4}\sin\frac{3\theta}{2}\right],$$

E_0 and ν_0 are Young's modulus and Poisson's ratio at the crack tip, respectively. As shown in this paper, the higher-order terms of the series solution must be considered to adequately describe the stress field around the crack tip in FGM. The influence of higher-order terms can be considered in the formulation as a correction factor which is computed as the difference between the two-term solution and the higher order solution. The correction factor evaluated using eight-terms of the series is applied to the measured strain to obtain the corrected strains, $\tilde{\epsilon}_{rr}$ and $\tilde{\epsilon}_{\theta\theta}$, from which the SIF values can be computed as

$$\begin{Bmatrix} K_{\mathrm{I}} \\ K_{\mathrm{II}} \end{Bmatrix} = E_0\sqrt{2\pi r}\begin{bmatrix} \left(f^{\mathrm{I}}_{rr} - \nu f^{\mathrm{I}}_{\theta\theta}\right) & \left(f^{\mathrm{II}}_{rr} - \nu f^{\mathrm{II}}_{\theta\theta}\right) \\ \left(f^{\mathrm{I}}_{\theta\theta} - \nu f^{\mathrm{I}}_{rr}\right) & \left(f^{\mathrm{II}}_{\theta\theta} - \nu f^{\mathrm{II}}_{rr}\right) \end{bmatrix}^{-1} \begin{Bmatrix} \tilde{\epsilon}_{rr} \\ \tilde{\epsilon}_{\theta\theta} \end{Bmatrix}. \tag{B3}$$

The radial and hoop strains are measured by mounting a biaxial strain rosette near the crack tip. The strain gage must be located in the region prescribed by $r \geq 0.5B$, where B is the thickness of the specimen, for plane stress condition to prevail. Within this zone, r and θ must be chosen such that the coefficient matrix in the above equation is well conditioned and the sensitivity of measurement is maximized. For most common values of ν, the angles from 85 to 100° provide best conditioning of the matrix and peak strains occur in the neighbourhood of $\theta = 90°$ as shown in Ref. (Marur and Tippur, 1999). Hence, the strain rosette is mounted at $r = 0.6B$ and $\theta = 90°$ on the compliant side of the specimen.

References

Atkinson, C., List, R.D., 1978. Steady state crack propagation into media with spatially varying elastic properties. International Journal of Engineering Science 16, 717–730.

Delale, F., Erdogan, F., 1983. The crack problem for a nonhomogeneous plane. Journal of Applied Mechanics 50, 609–614.

Dhaliwal, R.S., Singh, B.M., 1978. On the theory of elasticity of a non-homogeneous medium. Journal of Elasticity 8, 211–219.

Eischen, J.W., 1987. Fracture of nonhomogeneous materials. International Journal of Fracture 34, 3–22.

Erdogan, F., 1995. Fracture mechanics of functionally graded materials. Composites Engineering 5, 753–770.

Erdogan, F., Wu, B.H., 1993. Analysis of FGM specimens for fracture toughness testing. In: Ceramic Transactions: Functionally Gradient Materials, American Ceramic Society, Westerville, Ohio, vol. 34, pp. 39–46.

Gu, P., Asaro, R.J., 1997a. Cracks in functionally graded materials. International Journal of Solids and Structures 34, 1–17.

Gu, P., Asaro, R.J., 1997b. Crack deflection in functionally graded materials. International Journal of Solids and Structures 34, 3085–3098.

Honein, T., Hermann, G., 1997. Conservation laws in nonhomogeneous plane elastostatics. Journal of Mechanics and physics of Solids 45, 789–805.

Jin, Z.-H., Noda, N., 1993. An internal crack parallel to the boundary of a non-homogeneous half plane under thermal loading. International Journal of Engineering Science 31, 793–806.

Jin, Z.-H., Noda, N., 1994. Crack tip singular fields in nonhomogeneous materials. Journal of Applied Mechanics 61, 738–740.

Jin, Z.H., Batra, R.C., 1996. Some basic fracture mechanics concepts in Functionally graded materials. Journal of the Mechanics and Physics of Solids 44, 1221–1235.

Marur, P.R., 1999. Fracture behaviour of functionally graded materials. Ph.D. Dissertation, Mechanical Engineering, Auburn University, Auburn, Alabama.

Marur, P.R., Tippur, H.V., 1998. Evaluation of mechanical properties of functionally graded materials. Journal of Testing and Evaluation 26, 539–545.

Marur, P.R., Tippur, H.V., 1999. A strain gage method for determination of fracture parameters in bimaterial systems. Engineering Fracture Mechanics 64, 87–104.

Niino, M., Hirai, T., Watanabe, R., 1987. Journal of Japan Society of Composite Materials 13, 257–264.

Rice, J.R., 1988. Elastic fracture mechanics concepts for interface crack. Journal of Applied Mechanics 55, 98–103.

Smelser, R.E., Gurtin, M.E., 1977. On the *J*-integral for bimaterial bodies. International Journal of Fracture 13, 382–384.

Tohgo, K., Sakaguchi, M., Ishii, H., 1996. Applicability of fracture mechanics in strength evaluation of functionally graded materials. JSME International Journal, Series-I 39, 479–488.

Yang, W., Shih, C.F., 1994. Fracture along an interlayer. International Journal of Solids and Structures 31, 985–1002.